

Watching Ultrafast Barrierless Excited-State Isomerization of Pseudocyanine in Real Time

Benjamin Dietzek[†] and Arkady Yartsev*

Department of Chemical Physics, Lund University, P.O. Box 124, 22100 Lund, Sweden

Alexander N. Tarnovsky

Department of Chemistry and The Center for Photochemical Science, Bowling Green State University, Bowling Green, Ohio 43403

Received: October 2, 2006; In Final Form: February 21, 2007

The photoinduced excited-state processes in 1,1'-diethyl-2,2'-cyanine iodine are investigated using femtosecond time-resolved pump–probe spectroscopy. Using a broad range of probe wavelengths, the relaxation of the initially prepared excited-state wavepacket can be followed down to the sink region. The data directly visualize the directed downhill motion along the torsional reaction coordinate and suggest a barrierless excited-state isomerization in the short chain cyanine dye. Additionally, ultrafast ground-state hole and excited-state hole replica broadening is observed. While the narrow excited-state wavepacket broadens during pump–probe overlap, the ground-state hole burning dynamics takes place on a significantly longer time-scale. The experiment reported can be considered as a direct monitoring of the shape and the position of the photoprepared wavepacket on the excited-state potential energy surface.

Introduction

Photoinitiated isomerization, one of the simplest yet most general reactions, is of great relevance in biology, for example, the first step in vision is a photoinduced isomerization of the retinal chromophore.^{1,2} Furthermore, it is the key process employed in the design of novel photoswitchable devices.³ 1,1'-Diethyl-2,2'-cyanine iodine (pseudocyanine, 1122C) belongs to the class of polymethine dyes that serve as model compounds in understanding the details of photoinduced excited-state isomerization⁴ and have therefore attracted much interest. Besides, their capability of forming extended aggregates^{5–8} stimulated extensive research in understanding exciton dynamics in large artificially aggregated systems. Very recently, theoretical and experimental efforts were undertaken to unravel the mechanism of adaptive feedback control of photoinduced barrierless excited-state isomerization employing cyanines as model compounds.^{9–14} Barrierless isomerization is a well-synchronized process with a pronounced driving force and directionality, having with the retinal isomerization crucial for vision an important biological example.^{1,2}

Recently, an extensive study of a different cyanine dye with the quinoline heterocyclic end groups in the 4,4'-position, 1,1'-diethyl-4,4'-cyanine iodide (1144C) was performed. In this molecule, isomerization was found to be a fast and viscosity-dependent barrierless process^{15,16} and transient states were observed by means of fluorescence up-conversion.¹⁷ Generally, it is a matter of discussion how universal or unique the barrierless character of the torsional motion on the excited-state PES is for 1144C,¹⁸ and it is questionable to deduce the shape of the excited-state PES of pseudocyanine from that of the structurally related system 1144C. However, having established a barrierless excited-state isomerization to occur in two similar

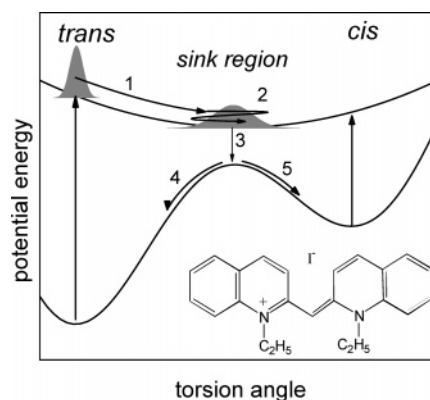


Figure 1. Schematic view of the one-dimensional model describing barrierless excited-state isomerization (for details see text). Inset: chemical structure of 1,1'-diethyl-2,2'-cyanine iodine.

yet structurally distinct molecules, these systems could be employed to study dynamic features of solvent viscous friction. This dynamic characterization will be possible, as for these systems different spatial rotational trajectories of the bulky end groups can be expected; a motion that can be correlated to the specific solvent microfriction, which determines the overall excited-state isomerization (ESI) process.

A one-dimensional model for barrierless ESI is schematically depicted in Figure 1. Upon photoexcitation of a cyanine dye molecule in its thermodynamically stable trans configuration with a short laser pulse, a wavepacket is created on the potential energy surface of the excited singlet S_1 state,¹⁹ leaving a ground-state hole in the population remaining on the ground state (S_0). While the ground-state hole is broadened, the excited-state population spreads and propagates for torsional motion toward the minimum of the excited-state potential (process 1). There a quasi-stationary population distribution is formed. It is characterized by individual molecules undergoing random (Brownian) walks along the torsional coordinate, while the center of the torsion-angle distribution remains constant (process 2), according

* Corresponding author. E-mail: arkady.yartsev@chemphys.lu.se. Tel: 0046-46-2220865. Fax: 0046-46-2224119.

[†] Current address: Department of Chemistry, Massachusetts Institute of Technology, 77 Massachusetts Avenue, Cambridge, MA 02139.

to the long standing theory of excited-state isomerization proposed by Bagchi, Fleming and Oxtoby (BFO).^{20,21} The appearance of process 2 is strongly dependent on the solvent friction; while in low friction solvents it is clearly present, it can be vanished in solvents of high friction.^{16,20,21} In the so-called sink region of the excited-state potential minimum, at which the energy gap between S_1 and S_0 potential energy surfaces is at a minimum, molecules undergo nonradiative transition back to the ground state (process 3). On the ground state potential molecules either relax back to the thermodynamically more stable trans configuration or form the cis photoisomer. Thus, the decay of the excited state as indicated in Figure 1 (process 3) leads to the trans-ground-state recovery (process 4) and the formation of the cis photoisomer (process 5). Though recent theoretical papers^{9–11} indicate that the one-dimensional model is a simplification of an in general more complex more-dimensional process, the experimental results presented in this contribution can be understood in the one-dimensional framework outlined here.

The overall process of ESI is characterized being a fast and solvent viscosity-dependent reaction, and the isoviscosity method can reveal the temperature dependence of the reaction rate. The latter shows very distinct features, consistent with the BFO theory.^{20,21} Nonetheless, these approaches are somehow indirect measures of the presence or absence of a barrier within the reaction path. Ideally, experiments need to be performed that allow for a real time monitoring of the system's downhill motion on the excited-state potential energy surface (PES). As the S_0 -potential in cyanines is typically much steeper along the reaction coordinate than the PES of higher excited states,⁹ the most straight forward approach to directly observe the isomerization reaction is monitoring of the spectral-temporal emission characteristics of the system. Such approaches will allow going considerably beyond typical start–stop reaction types, in which the photophysics of systems is interrogated that quickly after photoexcitation move out of a region of the potential energy surface accessible by electronic transitions. Thus, large portions of the overall reaction remain inaccessible and after initiation only the end point of the reaction is probed by—for example—the rise of the photoisomer absorption or ground state recovery. Such approaches have been frequently used to investigate the effect of solvent friction on isomerization.²²

In this paper, we consider the ESI of pseudocyanine, a system whose X-ray structure exhibits a distorted trans configuration in the crystalline state,²³ which is found to be practically nonfluorescent in low viscosity solvents^{24,25} and for which early picosecond time-resolved photoinduced absorption experiments revealed the existence of a photoisomer.^{26–28} The experiments presented here allow for a direct visualization of the system's downhill motion in real time, directly showing that excited-state torsional motion of 1122C in condensed phase occurs barrierless. Thus in correlation with the barrierless isomerization found in 1144C they open a doorway to investigate dynamic microfriction. Furthermore, it is shown that the excited-state motion can be separated into three distinct processes—namely, hole dynamics, torsional motion and nonradiative transition back to the ground state, processes presenting the core of ultrafast dynamics. While these processes among others dominate the photophysical properties of polyatomic systems in general, their interplay and temporal order will be dissected in detail for the excited-state isomerization of pseudocyanine.

Experimental

The femtosecond transient absorption spectrometer used in this work has been described elsewhere in detail.²⁹ An optical

parametric amplifier (TOPAS) was used as a pump source. Transient absorption (ΔA) kinetics at different probe wavelengths were measured by moving a variable optical delay in the path of the pump light while keeping the monochromator settings constant. The time-resolved spectra were measured by fixing a particular delay time between pump and probe pulse and subsequent scanning of the monochromator wavelength over the spectral range of interest. Because of the chirped white-light supercontinuum, chirp correction is needed. Subsequent to scanning the monochromator wavelength over the spectral range of interest, the delay line was moved in accordance with the predetermined chirp curve. The latter was obtained by measuring the delay of the apparatus response function for a set of probe wavelengths by means of sum-frequency generation at the sample position. This procedure allows us to measure chirp-free time-resolved spectra at the appropriate delay times between pump and probe pulse. The apparatus response function exhibited a Gaussian fwhm of ~ 200 fs for $\lambda_{\text{probe}} < 450$ nm and ~ 150 fs for $\lambda_{\text{probe}} > 450$ nm.

The transient absorption experiments were performed under magic angle polarization conditions. Typical sample absorbance for kinetic measurements was $A = 0.6$ at the excitation wavelength of 523 nm, while it was less than 0.3 when recording the differential absorption spectra. Homogeneous excitation conditions over the entire spatial area of the probe pulse was ensured by setting the diameter of the pump and probe beams to 270 and 110 μm , respectively. To avoid population to be transferred to highly excited states within the excitation as well as sample degradation, the excitation energy was kept below 0.4 μJ per pulse. Linearity of the photoinduced absorption signals with decreasing excitation intensity was ensured. For the determination of the quantum yield of isomerization, an optically thin sample was chosen with $A = 0.17$ at the excitation wavelength, and the excitation energy was kept slightly below 180 nJ per pulse.

1,1'-Diethyl-2,2'-cyanine iodine and methanol were purchased from Aldrich and Merck, respectively, and used without further purification. Absorption spectra were recorded before and after each experiment using a Jasco V-530 UV–vis spectrophotometer to ensure the integrity of the sample. The steady-state fluorescence spectra were acquired with a SPEX Fluorolog 2 spectrofluorimeter and corrected for the monochromator and photomultiplier efficiencies.

Results

Figure 2 displays the steady state absorption and fluorescence spectra of 1122C dissolved in methanol. The absorption and fluorescence transitions in the visible spectrum are both due to $\pi-\pi^*$ transitions, which are located on the cyanine chain. The main absorption is located at 523 nm (19120 cm^{-1}) and accompanied by two vibronic shoulders at 490 and ~ 460 nm, corresponding to $20\,420$ and $21\,740\text{ cm}^{-1}$. The vibronic progression reveals an optically active vibration characterized by 1300 cm^{-1} wavenumbers most likely due to stretching vibrations involving the nitrogen–carbon bonds of the central methine bridge.³⁰ The maximum extinction coefficient of 1122C in methanol of $4.52 \cdot 10^4\text{ M}^{-1}\text{ cm}^{-1}$ estimated from the steady-state absorption spectra agrees with the value of $5.4 \cdot 10^4\text{ M}^{-1}\text{ cm}^{-1}$ published by Rentsch.²⁷ A qualitatively identical absorption spectrum is seen in the case of DDI (1,1'-diethyl-2,2'-dicarbocyanine iodide), a longer chain cyanine dye, but here the overall width (fwhm) of the transition (885 cm^{-1}) is drastically smaller than in the case of 1122C (2230 cm^{-1}), Figure 2. Furthermore, also the emission spectrum of DDI

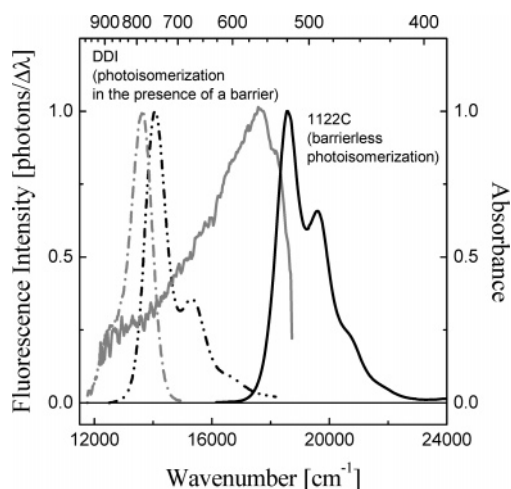


Figure 2. Absorption (black solid line) and corrected fluorescence spectra (gray solid line) of 1,1'-diethyl-2,2'-cyanine iodine (1122C) in methanol. The steady-state corrected fluorescence spectrum excited at 525 nm (19048 cm^{-1}), $c = 9.1 \times 10^{-6} \text{ M}$, and steady-state absorption spectrum, $c = 2.9 \times 10^{-5} \text{ M}$ of 1122C in methanol at room temperature. Steady-state fluorescence spectrum was obtained in a 10-mm quartz cell with a SPEX-Fluorog-2 fluorescence spectrometer working with a spectral bandpass of 5 nm both for excitation and emission. The steady-state spectra (dashed lines) of 1,1'-diethyl-2,2'-dicarbocyanine iodine (DDI) are shown for comparison. All the fluorescence spectra were corrected for the monochromator transmittance and photomultiplier response.

exhibits a smaller width and—opposing the characteristics of 1122C—represents an approximate mirror image of the absorption spectrum. The small bandwidth and the structured shape of the DDI fluorescence points to a bound excited state S_1 potential and the mirror-imaged emission indicates that only minor geometrical changes occur between the absorptive and emissive state, consistent with the previous laser photolysis

study.³¹ In contrast to DDI, the 1122C-emission does not represent a mirror image of the absorption spectrum and is found to appear significantly more Stokes-shifted, broad (3390 cm^{-1}) and featureless. Taken together, already the observation of the unstructured, broad emission and the large Stokes shift hint to severe changes during the relaxation from the absorption to the emission geometry in 1122C.

To characterize the overall temporal and structural changes leading from the absorption to the emission geometry in the photoexcited sample in detail, the differential absorption spectra of pseudocyanine dissolved in methanol were measured for various delay times (Figure 3). For short times, i.e., between -200 and -50 fs and thus in the range of pump–probe overlap, narrow spectral features are observed on either side of the excitation wavelength ($\sim 523 \text{ nm}$). Negative differential absorption signals are observed at 490, 525, 575, and 620 nm, while contributions of photoinduced absorption can be seen at 685 and 730 nm. The features at 525 nm and longer wavelengths are washed out at about -50 fs and thus on a time-scale shorter than the excitation pulse duration, which can be estimated from the experimental response function to be $\sim 100 \text{ fs}$. In contrast, the dip at 490 nm remains visible in the ΔA spectra up to delay times of about 200 fs.

Another important manifestation of the spectral dynamics is the position of the $\Delta A = 0$ points for various delay times, which appear due to the interplay of ground-state bleach (GSB) and stimulated emission (SE) contributions on one hand and excited-state absorption (ESA) on the other hand. With increasing delay time a zero signal wavelength shifts toward red from about 700 nm at -50 fs to approximately 1000 nm at 500 fs (inset of Figure 3C). At even later time, it is probably located at wavelength greater than 1000 nm, i.e., outside our range of probe wavelengths. For delay times longer than approximately 4 ps, no further shift of the $\Delta A = 0$ points is observed (Figure 3D, inset), and the ΔA spectra appear to decay homogeneously with

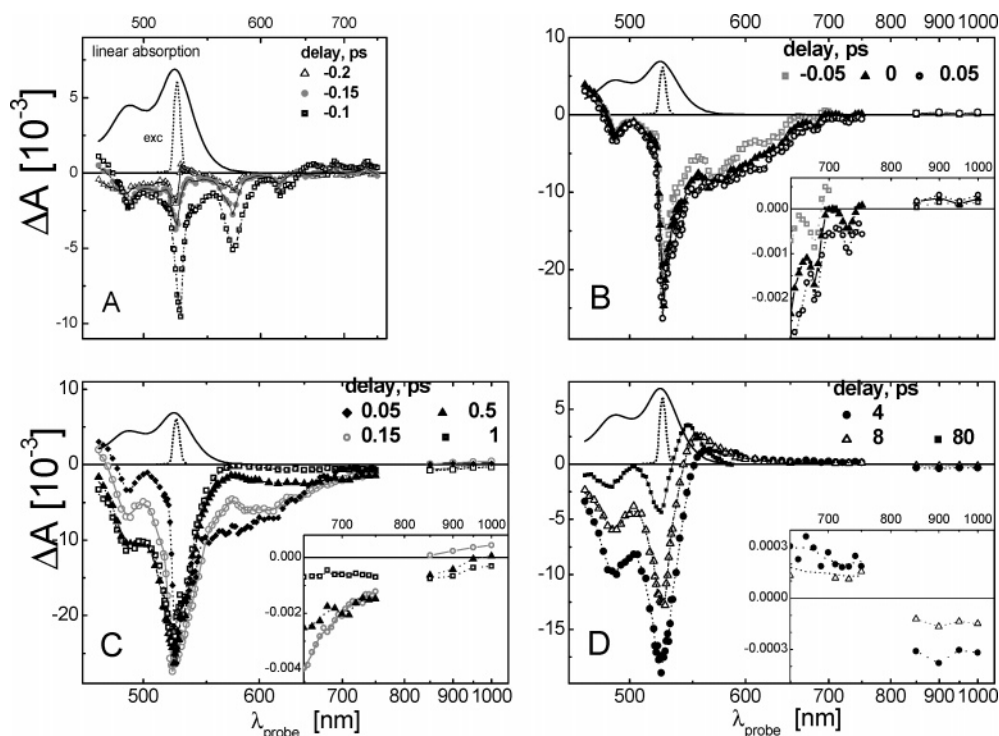


Figure 3. Differential absorption spectra of 1122C dissolved in methanol for various delay times (see legends) are shown in concert with the steady-state absorption spectrum of the stable ground-state isomer (solid line) and the spectrum of the excitation pulse (dashed line). Insets: enlarged view of the near-infrared part of the differential absorption spectra. In the spectral range from 750 to 850 nm, the fundamental of the laser interfered with probe light generation and prohibited us from obtaining reliable data.

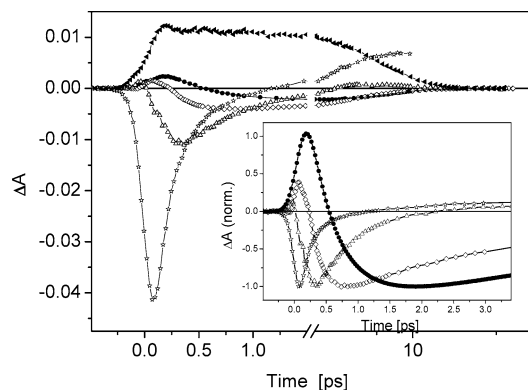


Figure 4. Representative transient absorption kinetics are shown for various probe-wavelengths. Inset: Short time behavior of kinetics measuring stimulated emission dynamics. The traces are normalized at the maximum negative differential absorption signal. Probe wavelengths: 405 nm (filled triangles), 573 nm (open stars), 700 nm (open triangles), 850 nm (open squares), and 1000 nm (filled circles).

increasing delay time. The differential absorption spectra obtained for long delay times (80 ps) demonstrate the formation of the photoisomer with the absorption spectrum red-shifted relative to the initial trans configuration. The spectral positions of the maxima in the 80 ps ΔA spectrum resemble those of the differential absorption spectrum obtained immediately after 20 ps excitation at 525 nm.²⁷ To unravel the contributions of the different processes such as ESA, SE, and GSB to the overall signals, kinetic traces recorded at probe wavelengths between 400 and 1000 nm are discussed in the following.

The dynamics of the overall excited-state population can be directly monitored by recording the ESA at around 400 nm, a spectral region where it is not contaminated by contributions from GSB or SE. As the ESA from the S_1 state is possible to a multitude of higher lying S_n states (originating from the higher density of states with increasing energy), it is less sensitive to the position of the wavepacket on the excited-state potential than SE. Hence, a less complex transient behavior of the ESA is expected, reflecting the evolution of the number of spectroscopically accessible excited molecules as a function of delay time. The corresponding kinetics (Figure 4) exhibits an experimentally limited rise and is subsequently found to remain flat for about one picosecond—the time-scale of motion from the Franck–Condon point of excitation to the bottom of the excited-state potential.^{20,21} Subsequently, the population in the excited-state starts to decay with a time constant of about 4.9 ps reflecting the dynamics of Brownian torsional motion at the bottom of the excited-state potential and nonradiative transition back to the ground state. This excited-state lifetime is in good agreement with the fluorescence lifetime estimate given by Keary and co-worker.³²

The main focus of this paper, however, is to detail the dynamics of SE, directly reflecting the motion of the photoexcited wavepacket on the excited-state potential. The contribution of ESA to the kinetics recorded in the visible spectral range can be estimated from the short-delay time differential absorption spectra (see Figure 3) to be in the order of $5 \cdot 10^{-4}$. Hence, ESA is contributing much less to the overall signal than SE, which is manifested in the kinetics measured for wavelengths longer than 523 nm as a negative contribution. It is evident that the maximum in the SE kinetic traces appears more strongly delayed when stimulated emission is probed further to the red from about 100 fs at 573 nm to 750 fs probed at 850 nm, for example, and whose subsequent decay is slowed in concert (Figure 4). The shift of the SE spectra associated with the kinetic

behavior discussed gives rise to the red shift of the $\Delta A = 0$ point over the first ps as described above (Figure 3). From the kinetic traces (Figure 4) it is evident that the oscillator strength of the SE drops with increasing probe wavelength. This effect appears even more pronounced when considering the intrinsic underestimation of the SE amplitude for the fast decaying kinetics due to the limited time resolution of the experiment. Under the assumption of only very minor ESA contributions to the observed differential absorption signals in the wavelength region between 575 and 1000 nm (as discussed above), the corrected amplitude ratio between the SE signals in that spectral region is estimated to be approximately 50. This decrease in oscillator strength of the stimulated emission results from the increasingly broken conjugation of the methine bridge due to the rotation of the quinoline groups as theoretically predicted in ref 33. To the best of our knowledge, the data presented here constitute the first experimental illustration of the transition dipole moment change of a molecule while it is undergoing excited-state bond-twisting motion.³⁴

Furthermore, the transients measured at short probe wavelengths (573 and 700 nm) exhibit a qualitatively different behavior than those recorded at longer wavelengths. At the short probe wavelengths photoinduced absorption takes over from stimulated emission for delay times longer than 1 ps. This can be attributed to the long-lived ESA extending from at about 400 nm into this spectral region, which dominates the signal when the SE contribution has decayed. In addition, the transient recorded at 573 nm detects the photoisomer absorption (see Figure 6). The photoisomer absorption can be seen at long times ($t > 10$ ps), while the decay of the positive differential absorption amplitude on a 10 ps time scale is correlated with the overall decay of the excited-state as measured by ESA at 400 nm (Figure 4). Moreover, good fits of the $\Delta A > 0$ rise at 573 nm can be achieved with the decay time of the ESA decay (data not shown).

The inset in Figure 4 presents the kinetics of the main panel after being normalized to their maximum negative amplitude, which enables to reveal different rise and decay components of the SE at various wavelengths. In order to analyze the data quantitatively, the kinetic traces were fitted to a multiexponential decay, which is not to prove any particular model, as the rise and decay of the transient species involved in the excited-state isomerization are not expected to follow simple exponentials.^{20,21} Nonetheless, the analysis will yield considerable insight in the excited-state wavepacket motion; it shows that the SE decay is slower and the corresponding rise component is getting more pronounced for longer probe wavelengths. Some multiexponential decay components of the blue part of the SE (for example the 250 fs decay at 573 nm, see Figure 5) correspond very well to the rise of the negative signal in the near IR (250 fs rise component at 850 nm). For probe wavelengths longer than 850 nm, the decay of the SE signal turns out to be single exponential and can be characterized by a time constant of 4.9 ± 0.2 ps. The reduction in the description of the SE decay for longer wavelengths than 850 nm (multiexponential behavior for $\lambda_{SE} < 850$ nm and monoexponential decay for $\lambda_{SE} \geq 850$ nm) indicates that a single process is dominant in this region, while for shorter probe wavelengths ($\lambda_{SE} < 850$ nm) additional processes contribute. From the excellent agreement of the 4.9 ps estimate obtained from fitting the $\lambda_{SE} \geq 850$ nm data with the time constant obtained for the decay of the ESA at 400 nm and the fluorescence lifetime reported,³² it is tempting to assign this process to the overall deactivation of the excited state. Thus, we conclude that probing the IR part of the SE signal gives

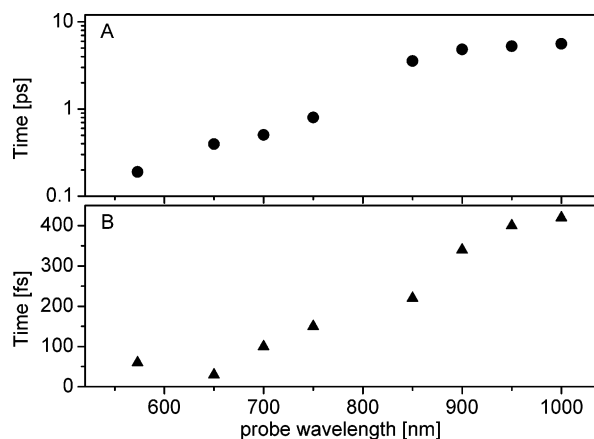


Figure 5. Decay (A) and rise components (B) of stimulated emission as obtained from fitting the kinetics at different probe wavelengths. Please note the logarithmic scale in panel A.

direct access to the kinetics of a quasi equilibrated excited-state population in contrast to probing motion of the wavepacket on the excited-state potential for bluer SE regions.

The result of the fitting procedure is summarized in Figure 5. Both the rise and decay component show a significant increase from about 50 to 420 fs and 0.2 to roughly 5 ps, respectively, when gradually shifting the probe to longer wavelengths. However, when plotting the time constants of the decay of the SE as a function of emission wavelength, the plot levels off for the probe wavelength approaching 1000 nm, indicating that a quasi equilibrated excited-state configuration is reached before excited molecules are deactivated. The quasi-equilibrated state is characterized by almost no changes in the center of the torsion angle distribution and its high-energy emission tail is observed at approximately 900–1000 nm. However, it should be noted that the reddest SE observed in our experiments does not correspond to emission from the sink region itself. At the sink region, the potential energy surfaces approach each other, and therefore their energetic separation tends to zero. Furthermore, the rise times of the 900–1000 nm SE is only about 400 fs (Figure 5B) and thus shorter than the onset of the ESA decay as monitored at 405 nm (Figure 4). Hence, the population emitting in the spectral region between 900 and 1000 nm has not arrived in the sink region, however the monoexponential 4.9 ps decay observed indicates that it constitutes the high-energy emission tail of a thermalized population. The deactivation of the arrested state occurs concertedly and thus a monoexponential decay of this state is observed. In line with refs 25 and 32 we suggest that the overall concerted decay of the near-infrared SE and the correlated ESA is due to Brownian torsional motion and radiationless transition of excited molecules back to the ground state (processes 2 and 3 in Figure 1). Subsequent to the radiationless transition, torsional motion takes place on the ground-state potential energy surface, resulting in the formation of the ground-state cis photoisomer and the partial recovery of the trans isomer.^{26–28}

In order to estimate the isomerization quantum yield, it is assumed that a single type of photoisomer molecules (cis configuration) is produced upon excitation of the stable trans isomer, so that $\Delta A(\lambda) = (-\epsilon_{\text{cis}}(\lambda) + \epsilon_{\text{trans}}(\lambda)) \cdot c \cdot l$, where Δc refers to the (identical) concentration changes of cis and trans molecules, ϵ_{trans} and ϵ_{cis} are the molar extinction coefficients, l is the sample path length, and λ is the probe wavelength. Subsequently, the differential absorption spectrum at 80 ps (Figure 3) was fit to a superposition of the original ground-state absorption and a similar absorption spectrum, but spectrally

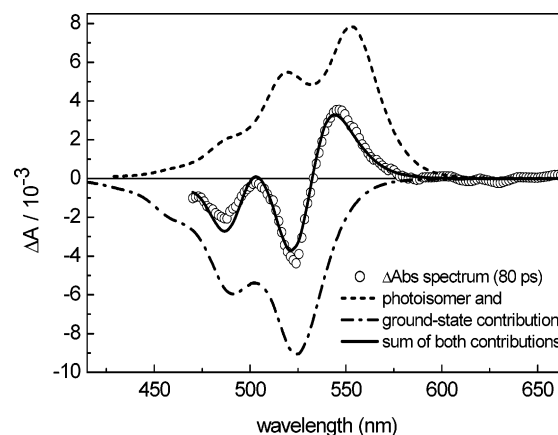


Figure 6. The result of the fit determining the photoisomer absorption spectrum is shown. Circles represent the experimentally determined differential absorption spectrum at 80 ps, while the dashed and dash-dotted lines refer to the contributions of photoisomer absorption and ground-state bleach, respectively. The solid line displays the outcome of the fit as the sum of the latter contribution. For details, see text.

shifted (in a representation plotting the transition dipole moment vs wavenumber) and scaled to represent the ground-state absorption of the photoisomer; the shift and scaling factor were fit parameters. Thereby, the maximum extinction coefficient of the isomer and the spectral shift between the trans isomer and the photoisomer absorption were estimated to be $3.72 \cdot 10^4 \text{ M}^{-1} \text{ cm}^{-1}$ (at 553 nm) and 533 cm^{-1} , respectively, Figure 6. Having ensured that the differential absorption spectrum is linearly dependent on the excitation energy, the number of cis and trans molecules contributing to the long-time ΔA spectra can be estimated. Hence, knowing the number of photons incident on the sample per pulse as well as the fraction of absorbed photons, the absolute isomerization quantum yield is calculated to be $27\% \pm 4\%$.³⁵ This agrees with the yield estimate of 30% based on the comparison of initial and residual GSB at 475 nm made by Rentsch.²⁷ However, the agreement seems fortuitous considering the difference between isomer extinction coefficient and the time resolution of the previous experiment (20 ps²⁷), which is considerably slower than the ground-state recovery (time constant, ~ 5 ps). However, a detailed discussion of the ground state processes is beyond the scope of this paper and will be discussed elsewhere.³⁶

Discussion—Watching Excited-State Relaxation

The results presented in this paper allow the overall excited-state relaxation to be decomposed into three different processes. This separation is not discrete in terms of time scales involved, as the processes overlap in time, but it appears straightforward in terms of characteristic spectral features and is highly instructive from a conceptual perspective. As shall be discussed in the following in more detail, the characteristic processes observed are (i) ground-state hole and excited-state hole replica broadening, (ii) torsional downhill motion of the broadened excited-state wavepacket, i.e., ESI, and (iii) formation of a quasi-equilibrated excited-state at about the perpendicular twisting angle, the geometry at which the radiationless transition back to the ground-state takes place.^{25,31,37,38}

(i) Upon photoexcitation, spectrally narrow differential absorption features are observed (Figure 3a) implying that the initial excitation leads to a localized rather narrow wavepacket on the excited-state potential energy surface, representing a replica of the ground-state hole burned by the excitation pulse. In detail, the narrow features are attributed to hole burning (0–1

and 0–0 transitions at 490 and 523 nm, respectively) and hole replica stimulated emission (negative differential absorption signals at 525, 575 and 620 nm) and hole replica absorption (photoinduced absorption signals at 685 and 730 nm). Interestingly, the ground-state hole observed at 490 and 523 nm is much longer lived than the stimulated emission features, which decay on the time-scale of less than 100 fs and thus within the pump-pulse duration (Figure 3c). The time-scale for ground-state hole broadening can be deduced from the plot of the HMHW (half-maximum half-width) measuring the blue side of the 0–0 transition hole at 523 nm as a function of delay-time (Figure 3c). For negative delay-times, the width appears to be nearly time-independent and its decay at positive times can be adequately fit to a single exponential with a time-constant of 200 fs, which is twice the upper estimate for the time of excited-state hole replica broadening. Hence, the data presented here show different time scales for the broadening of the hole and the hole replica, which is assigned to the different gradients of the potential energy surfaces of the ground and excited state.³⁹ As the ground-state hole is located at the bottom of the potential energy surface, the hole broadening is driven by thermal and therefore stochastic solvent reorganization only. However, the excited-state wavepacket is driven by the nonzero gradient of the potential. Thus, the broadening of the excited-state population results from the interplay of the directed torsional motion, which is opposed by the inhomogeneous local drag forces of the solvent.

(ii) The downhill motion of the ultrafast broadened excited-state wavepacket to the bottom of the potential energy surface is accompanied by geometrical changes in the molecules along the torsion coordinate, representing the relative orientation of the two quinoline rings with respect to each other.^{25,38} (The results obtained here with 200 fs time-resolution fit to the one-dimensional isomerization model.^{20,21} However, we are aware of recent theoretical work predicting a multidimensional potential energy surface being of relevance for the isomerization process.^{9–11}) The sink position in cyanine dyes corresponding to the geometry, in which the molecule undergoes nonradiative transition back to the ground state, is assigned to a strongly twisted geometry and thus in terms of conventional nomenclature about halfway (torsion angle $\varphi = 90^\circ$) between the trans and cis configurations.³³ According to BFO the distribution of the excited-state population in the sink region depends critically on whether the motion into the sink or the internal conversion is the rate-limiting step in the overall process.^{20,21} The study at hand establishes that for methanol and room temperature, the radiationless transition in concert with Brownian torsional motion close to the bottom of the excited-state potential turns out to be the rate-determining step. Prior to the deactivation of the excited-state population in the sink region a quasi-equilibrium is reached, which is reflected in the temporal behavior of the infrared SE transients presented in Figure 4. Under such circumstances, directed torsional motion on the excited-state potential can be separated from a random torsional motion in the sink region itself, where the center of the excited-state population is stationary and thus no spectral shift of the emission is observed any more. In contrast, directed ESI resulting in a shift of the center of the excited-state population can be directly followed experimentally by monitoring the spectrally resolved SE as a function of delay time.

The dynamics observed (Figure 4 and 5) can be accounted for, when assuming that SE at a particular wavelength is correlated with a particular portion of the excited-state potential surface, transiently populated during the excited-state twisting

motion. With this assumption it is straightforward to map the temporal shifts of the SE maximum onto the potential energy surface of 1122C. From Figure 5 it is obvious that both the motion into and out of a particular observation window (a particular position on the excited-state potential energy surface) proceeds gradually, monotonically, and monodirectionally. Furthermore, the data reveal that the shift of the excited state wavepacket slows down when the bottom of the excited state is approached. This behavior can be related to the reduced slope of the potentials and thus a minor driving force for the motion of the wavepacket close to the sink region. Thus, we can visualize that the excited-state isomerization of pseudocyanine is indeed barrierless.

It should be pointed out that other mechanisms such as a large photoinduced dipole moment change followed by solvation dynamics might lead to a Stokes-shift of the stimulated emission. However, the observed dramatic decrease in oscillator strength cannot be considered to be due to solvation dynamics alone, whereas it is in line with torsion motion.

(iii) Reaching the sink, a quasi-equilibrated state is formed, and spectral dynamics as reflected in the migration of the $\Delta A = 0$ points as discussed comes to a halt. Furthermore, this is manifested by the wavelength dependence of the decay components: The dependence of rise time constants upon probe wavelengths levels off for wavelengths longer than 850 nm (Figure 4). The depopulation of this quasi-equilibrated excited state can be characterized by the 4.9 ps monoexponential decay observed both in the transients at 400 and above 850 nm. Microscopically, the quasi-equilibrated state is characterized by random changes of the torsional angle in individual molecules, while keeping the center of the distribution constant at geometries corresponding approximately to the excited-state minimum, i.e., constant with respect to the sink position. As the plot of the SE rise time versus probe wavelength does not show the same flattening as observed for the decay component, we conclude that the longest probe wavelength (1000 nm) used in our experiment corresponds to the high-energy side of the emission of the quasi-equilibrated state. However, even longer probe wavelengths that would monitor the population dynamics closer to the sink region are expected to fall into the spectrally dark region.³³ Twisting ($\vartheta \rightarrow 90^\circ$) of a polymethine bond chain results in breaking of the conjugation chain, i.e., formation of two decoupled π fragments,³³ so that the oscillator strength of the emission from the sink region is drastically reduced as indeed reflected in the data (Figure 4). Therefore, the minimum of the excited S_1 state potential surface should be dark with respect to the emission process; nonetheless, by monitoring the high-energy emission of the quasi-equilibrated state at 1000 nm, the data reveal the dynamics of Brownian torsional motion and radiationless transition at the bottom of the excited-state potential.

Our experiments demonstrate that 1122C exhibits no excited-state barrier on the pathway from the initially excited Franck–Condon point to the metastable energy minimum on the S_1 -excited-state potential. However, the existence of an excited-state barrier cannot be completely ruled out as the experiments are performed at room temperature. Therefore, an alternative way of accounting for the observed spectral-temporal emission changes reads: Upon photoexcitation ultrafast hole broadening takes place. This process is followed by torsional downhill motion over a large range of torsion angles correlating with emission energies ranging over more than 9000 cm^{-1} . Finally, the excited state equilibrates on a 1 ps time scale. The arrested population remains in a meta-stable state with a lifetime of 4.9

ps close to the fully twisted 90° conformation. Having passed the small barrier a conical intersection is encountered leading to a rapid depopulation of the excited state. Such conical intersection has been calculated for a cyanine-model system to be displaced from the bottom of the excited-state and to be placed on the cis side of the potential.⁹ Hence, the 4.9 ps lifetime might reflect the presence of a small activation process, which separates the emissive state from the location of the conical intersection.

The data presented here constitute a detailed approach to a full characterization of the excited-state wavepacket downhill motion and directly visualize the time dependence of the molecular motion in the excited electronic S₁ state of pseudocyanine.

Conclusion

The photoinduced excited-state processes in pseudocyanine (1,1'-diethyl-2,2'-cyanine iodine) have been investigated by means of femtosecond time-resolved absorption spectroscopy. The results obtained show that (i) the overall excited-state relaxation can be separated into three distinct processes, hole replica broadening, directed excited-state torsional motion, and finally Brownian torsional motion in concert with radiationless transition back to the ground-state; (ii) it is proven that the torsional motion on the excited-state potential energy surface of 1122C occurs in a barrierless fashion. Furthermore, different time scales for ground-state hole and excited-state hole replica broadening are reported. Thus, the study at hand provides detailed insight in the processes of a paradigm light-induced reaction and constitutes a good starting point to more specifically investigate the interaction of the cyanine to its local environment and to approach a measurement of the local solvent friction at every single point of the potential energy surface. A detailed characterization of dynamic aspects of micro-friction in turn may lead to a more detailed understanding of the role of the evolutionary designed protein environments that host biological isomerizing light receptors and photoswitches and enable their function.

Acknowledgment. This work was financially supported by the Swedish Research Council. Many stimulating discussions with Villy Sundström are highly acknowledged.

References and Notes

- (1) Schoenlein, R. W.; Peteanu, R. A.; Mathies, R. A.; Shank, C. V. *Science* **1992**, 254, 412.
- (2) Kukura, P.; McCamant, D. W.; Yoon, S.; Wandschneider, D. B.; Mathies, R. A. *Science* **2005**, 310, 1006.
- (3) Bredenbeck, J.; Helbig, J.; Kumita, J. R.; Woolley, G. A.; Hamm, P. *Proc. Nat. Acad. Sci.* **2005**, 102, 2379.
- (4) Meyer, Y. H.; Pittman, M.; Plaza, P. *J. Photochem. Photobiol. A* **1998**, 114, 1.
- (5) Kopainsky, B.; W. Kaiser, W. *Chem. Phys. Lett.* **1982**, 88, 357.
- (6) Khairutdinov, R. F.; Serpone, N. *J. Phys. Chem. B* **1997**, 101, 2602.
- (7) Renge, I.; Wild, U. P. *J. Phys. Chem. A* **1997**, 101, 7977.
- (8) Kobayashi, T.; Nishimura, K.; Tokunaga, E. *J. Mol. Struct.* **2005**, 735–736, 179.
- (9) Sanchez-Galvez, A.; Hunt, P.; Robb, M. A.; Olivucci, M.; Vreven, T.; Schlegel, N. B. *J. Am. Chem. Soc.* **2000**, 122, 2911.
- (10) Hunt, P. A.; Robb, M. A. *J. Am. Chem. Soc.* **2005**, 127, 5720.
- (11) Improta, R.; Santoro, F. *J. Chem. Theory Comput.* **2005**, 1, 215.
- (12) Hoki, K.; Brumer, P. *Phys. Rev. Lett.* **2005**, 95, 168305.
- (13) Vogt, G.; Krampert, G.; Niklaus, P.; Nuernberger, P.; Gerber, G. *Phys. Rev. Lett.* **2005**, 94, 068305.
- (14) Dietzek, B.; Brüggemann, B.; Pascher, T.; Yartsev, A. *Phys. Rev. Lett.* **2006**, 97, 258301.
- (15) Åberg, U.; Åkesson, E.; Sundström, V. *Chem. Phys. Lett.* **1993**, 215, 388.
- (16) Alvarez, J. L.; Yartsev, A.; Åberg, U.; Åkesson, E.; Sundström, V. *J. Phys. Chem. B* **1998**, 102, 7651.
- (17) Yartsev, A.; Alvarez, J. L.; Åberg, U.; Sundström, V. *Chem. Phys. Lett.* **1995**, 243, 281.
- (18) Xu, Q. H.; Fleming, G. R. *J. Phys. Chem. A* **2001**, 105, 10187.
- (19) The term “wavepacket” is used within the one-dimensional model that only includes torsion angle as the reaction coordinate. Thus, the term “wavepacket” refers to the population placed on the excited state, which is distributed along the torsion coordinate. This spread along the reaction coordinate is due to the fact that finitely wide pulse spectra are used and the S₀–S₁ transition energy in the one-dimensional model is determined by the torsion angle of a given molecule. It should be stressed that the use of the term “wavepacket” in this publication does not refer to the superposition of vibrational levels.
- (20) Bagchi, B.; Fleming, G. R.; Oxtoby, D. W. *J. Chem. Phys.* **1983**, 78, 7375.
- (21) Bagchi, B.; Fleming, G. R. *J. Phys. Chem.* **1990**, 94, 9.
- (22) (a) Waldeck, D. H. *Chem. Rev.* **1991**, 91, 415. (b) Sension, R. J.; Repinec, S. T.; Szarka, A. Z.; Hochstrasser, R. M. *J. Chem. Phys.* **1993**, 98, 6291. (c) Awad, M. M.; McCarthy, P. K.; Blanchard, G. J. *J. Phys. Chem.* **1994**, 98, 1454. (d) Laitinen, E.; Ruuskanen-Järvinen, P.; Rempel, U.; Helemius, V.; Korppi-Tommola, J. E. *Chem. Phys. Lett.* **1994**, 218, 73. (e) Waldeck, D. H. *J. Mol. Liq.* **1993**, 57, 127.
- (23) Yoshika, H.; Nakatsu, K. *Chem. Phys. Lett.* **1971**, 11, 255.
- (24) Buettner, A. V. *J. Chem. Phys.* **1967**, 43, 1398.
- (25) Hofer, L. J. E.; Grabenstetter, R. J.; Wiig, E. O. *J. Am. Chem. Soc.* **1950**, 72, 203.
- (26) Rentsch, S. K.; Danielius, R. V.; Gadonas, R. A. *Chem. Phys. Lett.* **1981**, 84, 450.
- (27) Rentsch, S. K. *Chem. Phys.* **1982**, 69, 81.
- (28) Rentsch, S. K.; Danielius, R. V.; Gadonas, R. A.; Piskarskas, A. *Chem. Phys. Lett.* **1981**, 84, 446.
- (29) Kallioinen, J.; Benkö, G.; Sundström, V.; Korppi-Tommola, J.; Yartsev, A. *J. Phys. Chem. B* **2002**, 124, 4396.
- (30) Guo, C.; Aydin, M.; Zhu, H. R.; Akins, D. L. *J. Phys. Chem. B* **2002**, 106, 5447.
- (31) Razumova, T. K.; Tarnovsky, A. N. *Opt. Spectrosc.* **1995**, 78, 56.
- (32) Trendwell, C. J.; Keary, C. M. *Chem. Phys.* **1979**, 43, 307.
- (33) Momicchioli, F.; Baraldi, B. *Chem. Phys.* **1988**, 123, 103.
- (34) We thank the referee for pointing out the uniqueness of this experimental finding.
- (35) The absolute quantum yield of photoisomer (Φ_{iso}) following the ~100 fs excitation pulse at a 523 nm wavelength of 1122C in methanol was determined by the following expression:

$$\Phi_{\text{iso}} = \frac{\Delta A(545) \exp(t/\tau_{\text{iso}})}{\epsilon_{\text{PH}}(545) - \epsilon_{\text{NF}}(545)} N_A 10^{-3} \frac{F h \nu (\pi d^2/4)}{E(1 - 10^{-A(523)})}$$

Here, $\Delta A(545) = 1.6 \times 10^{-3}$, $\epsilon_{\text{PH}}(545) = 3.34 \times 10^4 \text{ M}^{-1} \text{ cm}^{-1}$, and $\epsilon_{\text{NF}}(545) = 1.59 \times 10^4 \text{ M}^{-1} \text{ cm}^{-1}$ are the transient absorbance, and the extinction coefficients of the photoisomer and trans-isomer all at the probe wavelength 545 nm, $E = 0.18 \times 10^{-6} \text{ J}$ and $F = 1.04$ are the incident excitation energy and its measured loss due to reflection off the cell front window, $A(523) = 0.17$ is the sample absorbance at the excitation wavelength, $h\nu = 3.797 \times 10^{-19} \text{ J}$ is the 523-nm photon energy, $N_A = 6.022 \times 10^{23} \text{ mol}^{-1}$ is the Avogadro number, and $d = 0.029 \text{ cm}$ is the “equivalent diameter” of the excitation beam at the sample position. The latter was calculated from transmission measurements of the excitation beam through pinholes for a set of varying diameters using the equation of Dietz and Merlin (Dietz, J.; Merlin, J. *J. Phys. C* **1987**, 48, 91.) as well it further confirmed by 2D Gaussian beam profiles measured using a linear diode array. The decay time of the photoisomer ground state (τ_{iso}) was measured to be 450 ps, and the term $\exp(t/\tau_{\text{iso}})$ was introduced because the quantum yield measurement was made at time $t = 80 \text{ ps}$ after excitation. The photoisomer quantum yield was calculated to be 0.27.

(36) Dietzek, B.; Tarnovsky, A. N.; Persson, P.; Yartsev, A. Manuscript in preparation.

(37) Dietz, F.; Rentsch, S. K. *Chem. Phys.* **1985**, 96, 145.

(38) Mialocq, J. C.; Jaraudis, J.; Goujon, P. *Chem. Phys. Lett.* **1981**, 84, 450.

(39) Ben-Amotz, D.; Harris, C. B. *Chem. Phys. Lett.* **1985**, 119, 305.